Autonomously Moving Local Nanoprobes in Heterogeneous Magnetic Fields

Prajnaparamita Dhar,[†] Yanyan Cao,[‡] Timothy Kline,[‡] Priya Pal,[†] Cheryl Swayne,[†] Thomas M. Fischer,*[,†] Brian Miller,[†] Thomas E. Mallouk,[‡] Ayusman Sen,[‡] and Tom H. Johansen[§]

Department of Chemistry and Biochemistry, The Florida State University, Tallahassee Florida 32306 4390, Department of Chemistry, The Pennsylvania State University, University Park, Pennsylvania 16802, and Department of Physics, University of Oslo, P.O. Box 1048, Blindern, Norway

Received: November 6, 2006; In Final Form: January 2, 2007

Different strategies of navigation in heterogeneous magnetic fields are investigated using natural and synthetic autonomously moving micro- and nanonavigators on top of a magnetic garnet film with uniaxial anisotropy creating a dense stripe domain structure. The use of ferromagnetic navigators leads to dynamic frustration, but synergy is achieved between the autonomous motion and magnetic orientation of paramagnetic navigators. The use of differently magnetized ferromagnetic and paramagnetic nanonavigators enables one to change from a roving to a guided motion. These different modes of motion can be utilized for distinct processes, such as the delivery and distribution of molecular cargo attached to synthetic navigators.

Introduction

Properly functioning nanomachines[1−4] operate in the unexplored realm of nanoscience. The motion of micro- and nanoscale objects is being used in nature for cell trafficking and the delivery of metabolized products. In nanoscience, one mimics strategies from nature and applies them to the nanoscale motion of roving sensors, drug delivery, and effective transport systems. Depending on the application, one tries to either guide the motion along well-established paths, or one uses a roving statistical motion for the fast spreading of components over a broad range. In either case, nanoshuttles on the colloidal scale[5,6] depend on reliable navigational data to fulfill their tasks in a usually heterogeneous environment. Navigational data will tell the nanoshuttles where they are, or where they should go, and will prevent the nanomachines from getting lost.

Here, we present a variety of autonomously moving natural and synthetic para- or ferromagnetic nanoshuttles[2] that respond with their orientation and motion to heterogeneous magnetic fields in their surroundings. We show that the motion of ferromagnetic magnetotactic bacteria and the motion of catalytic para- and ferromagnetic nanorods can be understood by controlling the relative strengths of their magnetism, their propulsion, and their thermal fluctuating properties. There is a surprisingly complex interplay of these interactions when the nanoshuttles are placed in a heterogeneous magnetic field on top of a magnetic garnet film. This allows us to continuously vary the motion from an enslaved guided motion, via a partially controlled anomalous diffusion, toward an autonomous statistical roving motion. While performing their autonomous motion, the navigators report information on the local direction of the magnetic field via the orientational order of their long axis. Catalytic nanorod and bacterial propulsion compete with the magnetic forces acting in the magnetic heterogeneities. The nanonavigator distribution in the heterogeneities is therefore dominated by the interplay of propulsion and orientation and significantly differs from an equilibrium Boltzmann distribution. The navigators are also able to sample the magnetic field in regions that are energetically unfavorable by multiples of the thermal energy. Four different nanoprobes, magnetotactic bacteria (*Magnetotacticum gryphiswaldense*), and three types of catalytic magnetic nanorods were released in an aqueous solution on top of a magnetic $Y_{2.5}Bi_{0.5}Fe_{5-q}Ga_qO_{12}$ ($q = 0.5-1$) garnet film where they moved according to the constraints set by the inhomogeneous magnetic field of the stripe domain pattern in the uniaxial anisotropy garnet film.

Experimental

Magnetotacticum Gryphiswaldense. Some of the most exciting magnetic navigators in nature are magnetotactic bacteria, which are guided by the geomagnetic field. *Magnetotacticum gryphiswaldense* (Figure 1 top) are bacteria of length 6.5 μm and diameter 0.7 μm that contain membrane-encapsulated vesicles (magnetosomes) filled with 40−100 nm Fe_3O_4 particles.[7] The vesicles are aligned along the long axis of the bacterium. The magnetic moment of the bacteria[8] is of the order $m \approx 1.5 \times 10^{-15}$ Am^2. The bacterium is propelled forward by flagella with a typical power[9] of $P \approx 10^4\ k_BTs^{-1}$. An oxygen concentration dependent forward or backward motion together with their magnetic nanocompass helps these bacteria to find their favored environment, the oxic/anoxic boundary layer[10] in the sediment at the bottom of lakes and rivers.

Synthetic Autonomous Magnetic Navigators. With our catalytic nanorods, we try to both mimic and vary the magnetic properties found in magnetotactic bacteria, but we use an entirely different propulsion mechanism. Three different structures were investigated for cylindrical nanorods.[2] Paramagnetic nanorods (type P nanorods, Figure 1) of diameter $2r = 400$ nm and length $l = 2.3$ μm are subdivided into two segments, one consisting of gold $l_{Au} = 0.9$ μm followed by another consisting of polypyrrole $l_{PP} = 1.4$ μm. The polypyrrole segment contains 5−20 nm diameter Fe_3O_4 particles.[11] Because of their smaller size as compared to the magnetite in magnetotactic bacteria,

* Corresponding author. E-mail: tfischer@chem.fsu.edu.
[†] The Florida State University.
[‡] The Pennsylvania State University.
[§] University of Oslo.

10.1021/jp067304d CCC: $37.00
Published on Web 02/10/2007

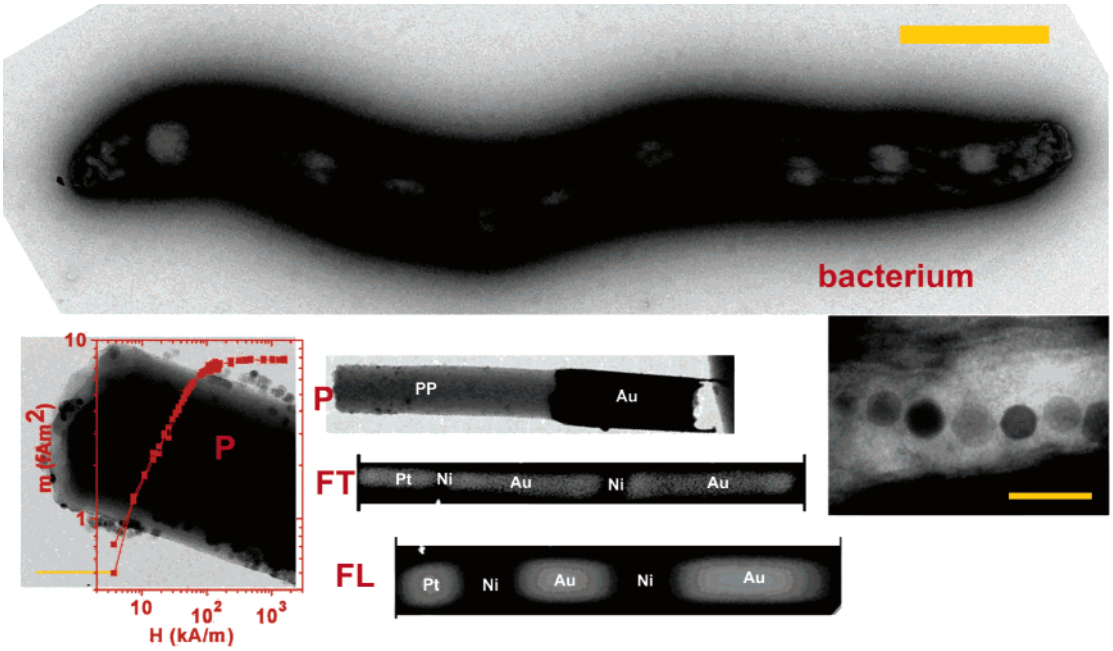

Figure 1. Electron micrographs (EM) of a magnetotactic bacterium (top) and of nanorods (bottom middle, type P, FT, and FL) showing the different segments of each rod. Bottom left: EM image showing a magnification of the polymer section of a type P rod containing Fe_3O_4 nanoparticles. A SQUID measurement of the magnetic moment of a type P rod versus the magnetic field showing the paramagnetic behavior of the rod is overlaid in the image. Bottom right: EM image showing a magnification of a magnetotactic bacterium highlighting a chain of vesicles (magnetosomes) that contain Fe_3O_4 nanoparticles. Scale bar (orange) corresponds to 100 nm for the high-resolution images to the bottom left and the bottom right; for the other images it corresponds to 1 μm.

the individual particles are superparamagnetic and their dispersed arrangement in the polypyrrole renders the entire rod paramagnetic (Figure 1). The rods have a saturation magnetic moment $m \approx 7.4 \times 10^{-15}$ Am^2 that is reached at an external magnetic field of the order of 100 kA/m. This is somewhat larger than the permanent magnetic moment of the magnetotactic bacteria.

Transversely and longitudinally magnetized ferromagnetic nanorods (type FT and type FL nanorods) of diameter $2r = 400$ nm and length $l = 2.6$ μm ($l = 2.5$ μm) are subdivided into segments consisting of platinum $l_{Pt} = 468$ nm ($l_{Pt} = 356$ nm) followed by nickel $l_{Ni,1} = 64$ nm ($l_{Ni,1} = 311$ nm), gold $l_{Au,1} = 957$ nm ($l_{Au,1} = 533$ nm), nickel $l_{Ni,2} = 106$ nm ($l_{Ni,2} = 444$ nm), and finally gold $l_{Au,2} = 1.021$ μm ($l_{Au,2} = 889$ nm) (Figure 1). The two nickel segments of the rod are ferromagnetic. Their size is chosen to be small enough to ensure that the nickel has a single ferromagnetic domain, but is large enough to suppress any superparamagnetic behavior. The type FT rods have nickel segments with an oblate geometry ($l_{Ni} \ll r$) and hence they favor the alignment of the nickel magnetization perpendicular to the rod (transversal magnetization). The type FL rods have prolate Ni segments with a magnetization pointing along the long axis (longitudinal magnetization). We use NdFeB magnets with a surface field of 0.48 T to magnetize the rods. The magnetization of the nickel segments is $M = 310$ A/m as estimated from the rod alignment in water in a magnetic field of $H = 1$ kA/m.[12] This magnetization is about one percent of the bulk-nickel magnetization making their magnetic moment about one percent of the magnetic moment of the magnetotactic bacteria. Previous experiments showed that the type FT (type FL) rods once magnetized, align with their long axis perpendicular (parallel) to a magnetic field.

The Fe_3O_4 particles in the type P rods and the platinum segment of the type FT and FL rods catalyze the oxidation of hydrogen peroxide H_2O_2 to oxygen and the gold segments catalyze reduction to water. The overall reaction (decomposition of H_2O_2 to oxygen and water) releases a Gibbs free energy of -50 k_BT per molecule at a reaction rate of typically 10^9 s^{-1}. A tiny fraction, 50 k_BT s^{-1}, of this power is used to propel the type P (FT and FL) rod in the direction of its polymer (platinum) end. Although several mechanisms may contribute to the propulsion of the nanorods[1,13,14] recent experiments with bimetallic nanorods of several different compositions suggest that the dominant contributor to the axial force is self-electrophoresis.[15] For the present discussion, it is sufficient to note that such rods move autonomously with velocities on the order of μm/s along their long axis in the direction of the polymer (platinum) end as long as they are not loaded (i.e., not located in a magnetic energy landscape). From the power of the rods, we can estimate that the force to stall the rods is of the order 50 k_BT/μm. The chemical propulsion mechanism dominates the longitudinal motion of the rods; however, orientation fluctuations govern the rotational motion. The superposition of the longitudinal and the rotational motion gives rise to an anomalous random walk[16] of the rods with a power law behavior of the center of mass autocorrelation function that is intermediate between normal diffusion and ballistic motion. This behavior is ideal if one wants the rod to sample a rich variety of sites, and thus cover a large area per unit time without sampling only a deterministic path.

Magnetic Garnet Films. The rods are dispersed in an aqueous 7% hydrogen peroxide solution and the bacteria are resuspended in a HEPES buffered solution (0.1 M, pH 7.0) containing ferric citrate (100 μM),[17] which is placed above a 4 μm thick magnetic garnet film of composition $Y_{2.5}Bi_{0.5}Fe_{5-q}Ga_qO_{12}$ ($q = 0.5-1$).[18] The film has a perpendicular spontaneous magnetization ($M_s = 11$ kA/m) with domains forming stripes alternating between up and down magnetization as shown in Figure 2.

A typical wavelength of the structure is around $\lambda = 2\pi/k \approx 10$ μm (i.e., larger than the length of the nanorods and on the

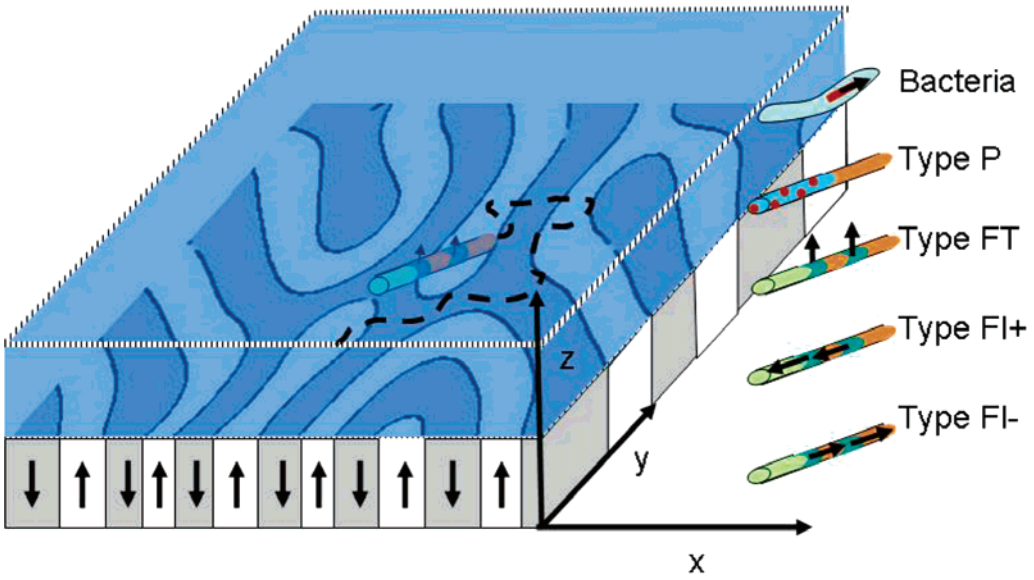

Figure 2. Scheme of a magnetic garnet film with upward (white) and downward (gray) magnetized domains forming a labyrinth pattern. Autonomously moving navigators (i.e., magnetotactic bacteria, paramagnetic or ferromagnetic rods of type P, FT, FL+, and FL−) are placed in an aqueous solution above the garnet film where they autonomously move. The orientation of the navigators is partially governed by the magnetic heterogeneities of the film and by orientational fluctuations.

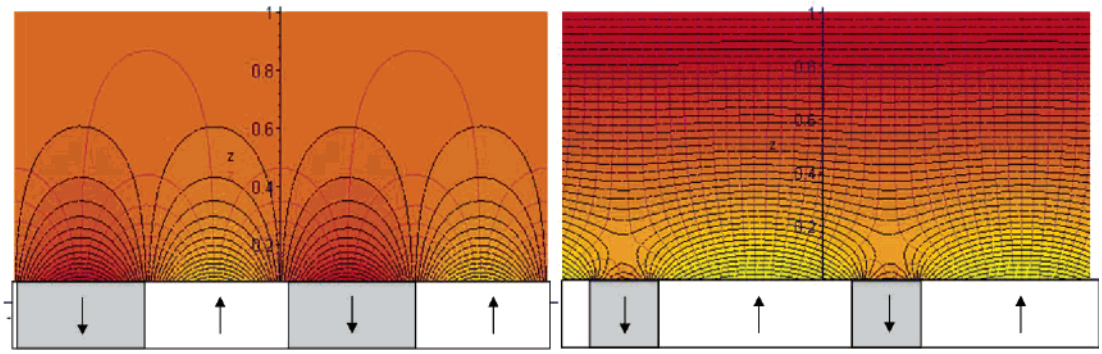

Figure 3. Equimagnetic potential (solid) and flux lines (shaded) above a striped garnet film with (left) no exterior magnetic field and (right) with a field of $H_{ex} = 0.6$ M.

order of the length of the bacteria). The stripes run in irregular directions with a persistence length of approximately 100 μm. All geometric parameters and the magnetization depend on the temperature, the value of q, or the presence of an external magnetic field H_{ex} perpendicular to the film.

Since the persistence length exceeds the size of the rod and the domain wall width is much smaller than the rod length, we use the limit of infinite persistence length and negligible domain wall width in the mathematical treatment of the problem. The magnetic field in this limit is purely two-dimensional and we write it as the gradient of a magnetic potential $\boldsymbol{H} = \boldsymbol{grad}\ \psi$, which is the real part of a complex function[19] $\psi = \mathrm{Re}(\Psi)$.

The equipotential surfaces are shown in Figure 3 (left and right) for vanishing external field $H_{ex} = 0$ and or $H_{ex} = 0.6$ M $= 6.5$ kA/m. Just above the magnetic film the equipotential planes are parallel to the surface above the domains and parallel to the yz plane above the domain walls. The magnetic field lines run perpendicular to the equipotential planes.

The nanonavigators sediment in the aqueous liquid due to gravity, but are repelled electrostatically from the garnet surface. Gravity and electrostatics efficiently confine the bacteria and the rods to a plane that is located a few nanometers above the surface of the garnet film. In Table 1 we list the ratio of the magnetic to the thermal energy E_m/k_BT, as well as the ratio of the propulsion power P to the product of the thermal energy and the shear rate γ. The thermal energies of the magnetotactic bacteria and rods are weak when compared with the magnetic and propulsion energies. The magnetic energy of the magnetotactic bacteria and of the type P rods is larger than the propulsion energy and the opposite is true for type FT and type FL rods.

TABLE 1: Magnetic and Propulsion Energies of the Navigators above the Garnet Film[a]

type	E_m/k_BT	$P/\gamma\ k_BT$
magnetotactic bacteria	4.6×10^3	5.5×10^3
type P	5.7×10^3	100
type FT	22	100
type FL	98	100

[a]Magnetic energies were calculated as $E = \mu_0 m M_s$, (μ_0 is the permeability of vacuum and M_s is the magnetization of the garnet film). The magnetic moment m is the permanent ferromagnetic moment for the ferromagnetic navigators, and the induced paramagnetic moment is taken from the SQUID measurement in Figure 1 at a field of $\boldsymbol{H} = M_s$. The propulsion energy is obtained by measuring the power $P = f\eta l v^2$ with $f \approx 20$ being the friction coefficient of the navigator, η is the viscosity of water, l is the length of the navigator, and v its velocity outside the magnetic field. $\gamma = v/l$ is the shear rate.

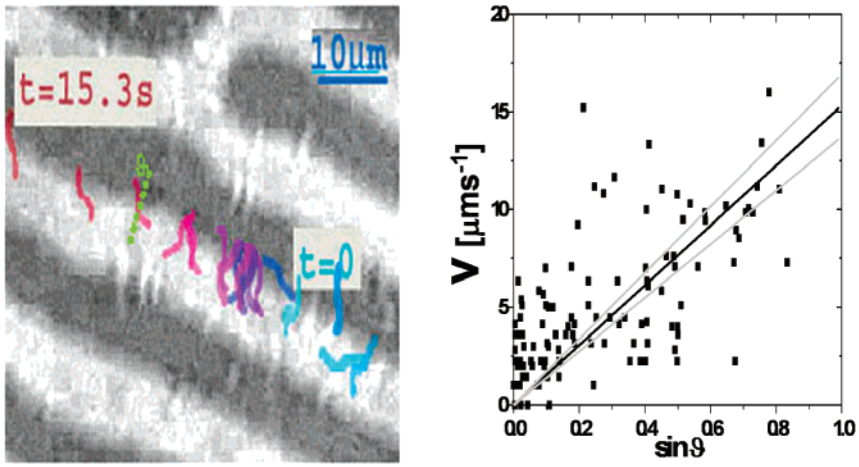

Figure 4. (left) Polarization microscope image of *Magnetotacticum gryphiswaldense* (bright) on a magnetic garnet film. Domains are visualized (crossed polarizer and analyzer) using the Faraday effect. A time sequence ($\Delta t = 0.9$ s) of the tangential motion of one bacterium (colored) along a domain wall is shown. (right) The velocity of the bacterium along the domain wall correlates with the projection of its director onto the stripe direction. A movie of the tangential motion of the bacteria may be viewed in the Supporting Information.

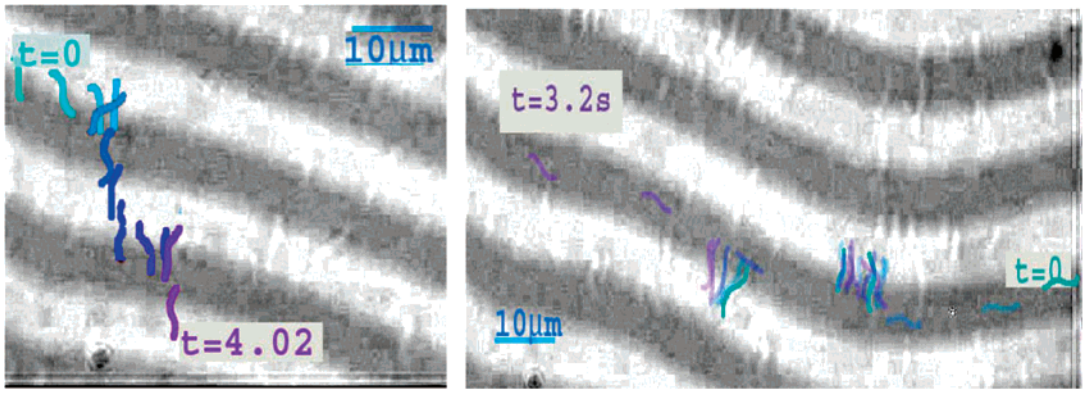

Figure 5. (left) Polarization microscope image of *Magnetotacticum gryphiswaldense* (bright) on a magnetic garnet film. A time sequence ($\Delta t = 0.3$ s) of the tangential motion, escape, recapture, and second escape from a domain wall of one bacterium (colored) is shown. (right) Two bacteria are trapped at the domain wall while one bacterium that has escaped to the dark domain avoids traveling antiparallel to the magnetic field by following the stripe direction. A movie of the trapped and guided bacteria may be viewed in the Supporting Information.

Results and Discussion

Magnetotactic Bacteria on Garnet Films. We first discuss the motion of magnetotactic bacteria on the garnet films; most of the bacteria are trapped at the domain boundaries. Figure 4 (left) shows an ensemble of north seeking bacteria (bright) trapped at the domain walls. A time sequence of the position of one bacterium, marked in color, is overlaid on an image of the garnet film. As one can see, there is vigorous motion induced by the flagella; however, the field of the domain wall is too strong to let the bacterium escape and its motion is confined to the domain wall. The tangential velocity is roughly proportional to the projection of the bacterial long axis onto the domain wall.

Occasionally a bacterium escapes the domain wall. Examples of two such events are shown in Figure 5. The direction of the magnetic field above a domain wall alternates between parallel and antiparallel. In Figure 5 (left), a bacterium trapped at a domain wall escapes and traverses the next domain wall, which has a magnetization direction antiparallel to the magnetosomes. The bacterium gets recaptured at the next domain wall, which has its magnetic field parallel to the magnetosome magnetization. After some time, the bacteria can escape again from this domain wall and across an apparently unfavorable domain wall. Surprisingly, it gets trapped at the apparent unfavorable domain wall. Kalmijn et al.[20] have shown that microsecond field pulses of the order 50 kA/m may remagnetize north seeking into south seeking bacteria. When the bacterium moves across a domain wall, it experiences a field pulse of slightly lower magnitude but longer duration at the domain wall and might get remagnetized. Presumably such a remagnetization occurred when the bacterium moved over the unfavorable wall. The unfavorable wall is turned into a favorable wall by this process, explaining the trapping. In Figure 5 (right) the bacterium avoids the domain wall and moves parallel to the stripe at high speed ($v = 27$ μm s^{-1}) because it is unable to penetrate the unfavorable domain wall. The only way the bacterium can align itself parallel to the field is to point downward, but this direction is blocked by the garnet surface. Going up or crossing the domain wall toward a bright domain would mean traveling antiparallel to the magnetic field and the bacterium avoids such motion by choosing the more favorable direction, that is perpendicular to the magnetic field (along the dark stripe). Thus while bacteria trapped at the domain walls undergo motion along the domain wall, a bacterium stuck in the dark domain travels along the stripe and perpendicular to the magnetic field.

The addition of magnetotactic bacteria on top of the garnet film guides the bacteria perpendicular to the magnetic field in contrast to their behavior under natural conditions. This guidance is achieved only for the small fraction of dynamically frustrated

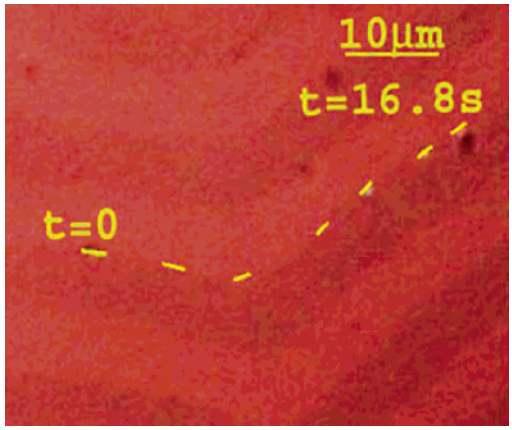

Figure 6. Overlay of polarization microscope images of a type P rod (yellow) on a magnetic garnet film. A time sequence ($\Delta t = 2.8$ s) of the motion along a domain wall of one rod ($t = 0-16.8$ s) is shown. A movie of guided nanorod may be viewed in the Supporting Information.

bacteria, namely those strong enough to escape the field gradient of the magnetic domain walls.

Strategies for Guided Motion of Synthetic Magnetic Nanonavigators. We may use the results from the bacteria motion for strategies of guided motion of synthetic magnetic nanonavigators. One might think of several strategies for achieving better guidance with magnetic nanorods. First, the ferromagnetic orientation is somehow in conflict with the desired propulsion direction. The magnetic field orients the majority of bacteria perpendicular to the stripe pattern, but we would like to guide them along the stripes. Guidance of the minority fraction is only achieved by dynamic frustration of the bacteria. One may resolve this conflict of orientation by using paramagnetic instead of ferromagnetic rods, which will always establish a magnetic moment in the direction of the magnetic field. This leaves the navigators more options to move in various directions. This strategy was followed with type P rods. Another strategy is to achieve a synergy between the rod motion and magnetism by orienting the magnetic compasses perpendicular to the long axis. In this case, the long axis lies along the domain wall of the garnet film, and the magnetic moment points parallel to the magnetic field of the domain wall. This strategy was followed by using type FT rods. Finally one might simply reduce the longitudinal ferromagnetic moment of the rods relative to that of the magnetotactic bacteria. This last strategy is implemented by using type FL rods. In the following, we discuss the success of these strategies.

Paramagnetic Rods on Garnet Films. Figure 6 shows a typical trajectory of an autonomously moving type P nanorod above the surface. In a field corresponding to the saturation magnetization M_s of the garnet film, the magnetic moment of the nanorod approximates that of the magnetotactic bacteria. The domain walls are again strong enough to trap most of the rods above the domain walls. However, because the direction of the magnetic moment is not fixed, the rods minimize their magnetic energy by placing all Fe_3O_4 nanoparticles directly above the domain wall in which the field is strongest. This allows the rods to orient parallel to the domain wall. Their motion is purely one-dimensional with the rods traveling along the path dictated by the domain walls. Hence, the strategy of using paramagnetic instead of ferromagnetic rods to obtain a higher fraction of navigators to travel along the domain walls was successful. In effect, all of the rods are guided by the garnet structure.

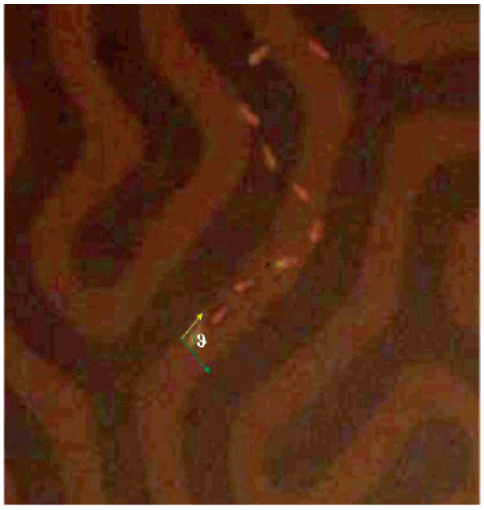

Figure 7. Polarization microscopy image of transversally magnetized type FT nanorods (bright) on a magnetic garnet film. A typical fractal trajectory of a nanorod is overlaid on the image. We also show the definition of the angle ϑ between the nanorod director **c** and the local **k** vector of the stripe pattern. A movie of the roving motion of the nanorod may be viewed in the Supporting Information.

Transversally Magnetized Ferromagnetic Rods on Garnet Films. Type FT rods are magnetized perpendicular to their long axis. Writing the magnetic field as the gradient of a magnetic potential $\boldsymbol{H} = \boldsymbol{grad}\ \psi$ demonstrates that the magnetic field confines the motion of type FT rods to a constant magnetic potential plane $\psi = \psi_0$. Type FL rods are magnetized along their long axis, and like the magnetotactic bacteria they prefer to follow the field lines of the magnetic field.

Figure 7 shows a typical trajectory of an autonomously moving type FT nanorod above the surface. Although the magnetic energy of the rod exceeds the thermal energy, the propulsion energy dominates the motion. The course follows a statistical fractal path that frequently crosses the stripes showing little correlation to the garnet structure. To extract the statistical correlation between the rod motion and the garnet structure, the probability density (f) of finding the rod at a certain distance s ($0 < s/\lambda < 1$) from a domain wall can be measured. Low s values correspond to dark stripes, while high s values correspond to bright stripes. In addition, we measure the time-averaged rod orientation $<\cos 2\vartheta>$ at this location and $\vartheta(-\pi/2 < \vartheta < \pi/2)$ is the angle between the long axis of the rod and the local k-vector of the stripe pattern (Figure 8a−f). The **k** vector is defined to point in the same direction as the normal component of the rod velocity. As the magnetic forces are small compared to the rod's stalling force, the absolute value of the rod velocity is constant. From the equation of continuity ($df/dt + div(f\mathbf{v}) = 0$) we conclude that the probability density (f) should be inversely proportional to the average speed, $\mathbf{v}_n = \mathrm{v}\cos\vartheta$, normal to the stripes (See Supporting Information for a detailed derivation)

$$f \propto < \frac{1}{\lambda|\cos\vartheta|} > \approx \frac{2}{\lambda\sqrt{1 + <\cos 2\vartheta>}} \qquad (1)$$

Figure 8a shows the orientation $<\cos 2\vartheta>$ of type FT rods versus s/λ for a zero external field. As expected, there is little preferred orientation above the domains, as the equipotential plane is parallel to the garnet surface. This allows the rod to orient equally well in either the x or y direction of the equipotential surface. However, above the domain walls the rod orients along the direction of the domain wall ($<\cos 2\vartheta> <$

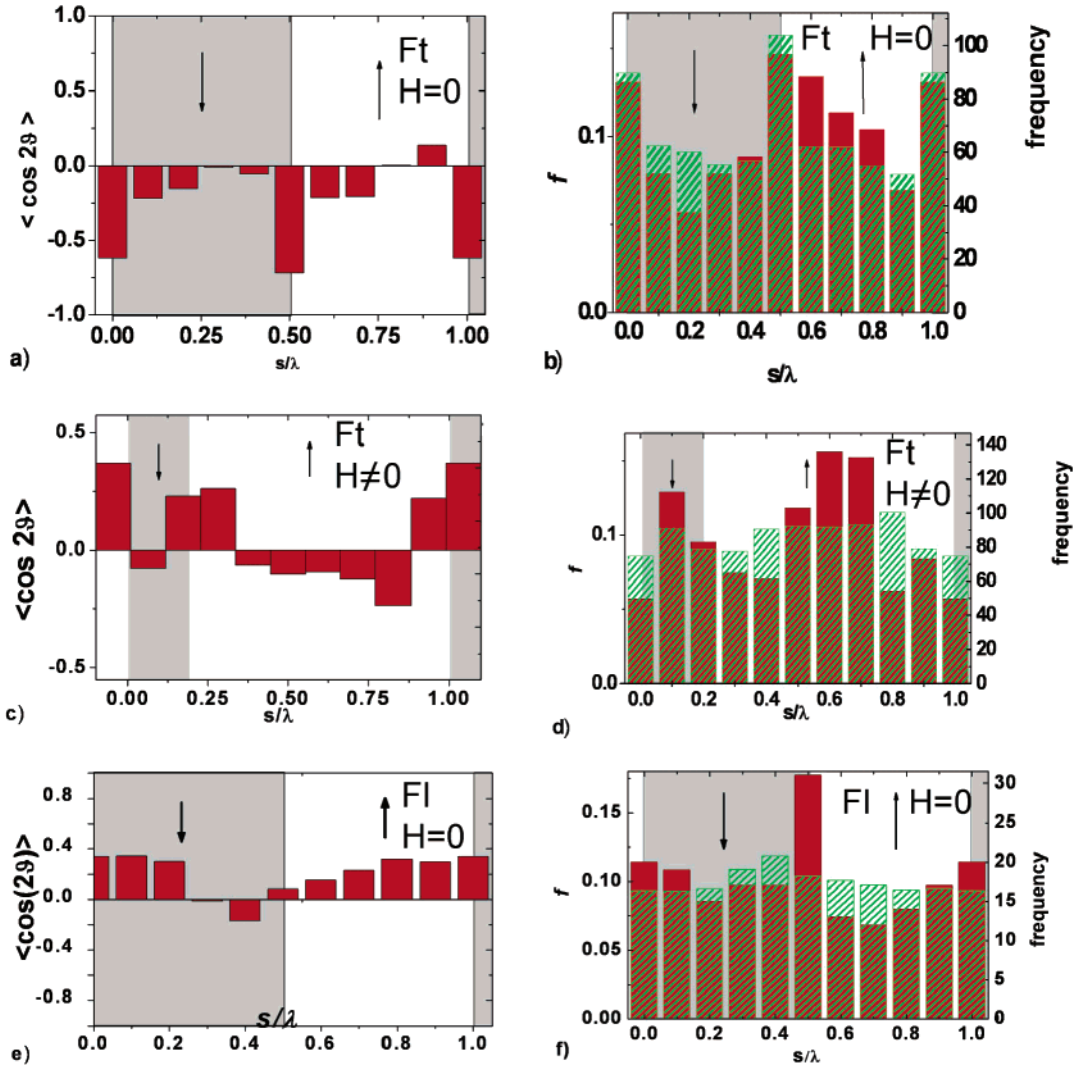

Figure 8. Panels a,c, and e show the plot of orientation $<\cos 2\vartheta>$ and panels c,d, and f show the probability density f of (i) type FT (a−d) and (ii) type FL (e,f) nanorods above the garnet film as a function of the position s/λ in the labyrinth. The data in panels a,b,e, and f are all in the absence of an external field, while panels c,d correspond to an external field of $H_{ex} = 6.5$ kA/m. The red data were obtained in a 7% aqueous H_2O_2 solution. The green crosshatched data of the probability density was calculated from the orientational data to the left via eq 1.

0), because the only direction of the equipotential plane that is parallel to the surface above the domain walls is normal to the **k** vector. In Figure 8b, we plot the probability density f versus s/λ. There is good agreement between the observed value of f and that calculated from eq 1 (red and green crosshatched data) indicating that the probability density is indeed a result of the orientation of the rod and its forward motion.

In Figure 8c,d, we again plot $<\cos 2\vartheta>$ and f but for motion with an applied external field of $H_{ex} = 6.5$ kA/m. The degree of orientation $<\cos 2\vartheta>$ of the rod above the domain walls is reduced as compared to the no external field ($H_{ex} = 0$) case. The field strength (the density of equipotential lines) above the domain walls for $H_{ex} = 0.6$ M is substantially reduced as compared to the no field situation, $H_{ex} = 0$ (Figure 3). The alignment parallel to the domain wall is therefore no longer enforced. The rods are less oriented and distributed more uniformly across the labyrinth structure (Figure 8c,d). However, there seems to be a slight preference for an orientation of the rods perpendicular to the domain walls. According to eq 1, this would result in a preference of the rods to reside in the interior of the domains as observed in Figure 8d. The preference for the stripe interior, however, appears to be larger (red columns) than what is expected on the basis of the orientational data (green crosshatched columns) in Figure 8c.

Longitudinally Magnetized Ferromagnetic Rods on Garnet Films. Figure 8e,f show similar data of type FL rods. The magnetic moment of type FL rods points either in (type FL+) or against (type FL-) the direction of the platinum end (this contrasts with magnetotactic bacteria, which are polarized in only one direction).[10] Their orientational order, therefore, substantially differs for the domain walls located at $s/\lambda = 0$ and $s/\lambda = 1/2$. Figure 8e shows the orientation of a type FL+ rod versus s/λ. The rod prefers to pass straight ($\cos 2\vartheta > 0$) over a $s = 0$ domain wall with the magnetic field oriented in the direction of motion. If the magnetic field above the domain wall is antiparallel to the direction of motion, then $s/\lambda = 1/2$ and we observe the rod passing over the domain wall at an oblique angle ($\cos 2\vartheta \approx 0$). Figure 8f shows the probability density f of the (type FL+) rods versus s/λ. We measure a minimum of f at $s/\lambda \approx 0$ and a maximum at $s/\lambda \approx 1/2$. The measurements are in concordance with the trend deduced via eq 1 from the orientational data (green crosshatched columns).

Equation 1 predicts a maximum at the domain wall where the rods have an oblique angle. Indeed, Figure 8e,f prove that

the distribution of rods above the heterogeneous garnet film is dominated by the autonomous motion, which does not require the rods to comply with the magnetic energy considerations.

The values of the magnetic field and magnetic moment of the rod are such that the magnetic orientational energy is smaller than the propulsion energy. The random distribution in Figure 8d (red columns) indicates that the motion of the rod eliminates the equilibrium behavior, and the location of the rod is dominated by autonomous motion rather than by magnetic energy.

Summary

Strategies for Roving Versus Guided Autonomous Motion Revisited. Surprisingly, the results suggest that guidance of the navigators is best achieved if they are paramagnetic and there is a synergy between the autonomous motion and the field guidance. If the magnetic energy is larger than the propulsion energy, ferromagnetic navigators are either trapped by the domain walls or the propulsion power of the rod engine overcomes the magnetic energy landscape easily. In the later case, there is only a mild correlation between the propulsion and the magnetic field direction. Moreover, the field direction is in conflict with the propulsion direction for longitudinally magnetized navigators. In the case of dominating magnetic energies, this leads to frustrated guidance of the minority fraction of freed magnetotactic bacteria along the stripe direction, and a trapping to the domain walls of the majority of bacteria. Conversely, when the propulsion energy dominates the rods are pushed away from the domain walls to the regions above the domains where for geometrical reasons the rods lose their orientation. Transversely magnetized rods have some preference for the domain walls, but the propulsion again overcomes the magnetic constraints leading to an overall statistical motion of these rods. From these considerations, it is clear that by adjusting the ratio of the propulsion versus the magnetic energy, one might switch from a roving to a guided shuttle. It is therefore desirable to identify magnetic nanoshuttles with tunable and stronger propulsion properties. Varying the propulsion power then would allow a switching between guided and roving motion simply by varying the amount of propellant and at the same time keeping both the magnetic as well as the propulsion energy well above the thermal energy. One might also use a paramagnetic to ferromagnetic transition to control the different modes of navigation. This might be done by changing the temperature or in some cases by photoexcitation. This would enable future magnetic nanoshuttles to be guided to a specific target,and then dispersed at will. Such navigators have the potential to find widespread application in drug delivery and distribution.

Acknowledgment. We acknowledge Geoffrey Strouse and Donny Magana for the SQUID measurements. Financial support from the NSF-MRSEC program, DMR-021362 is highly acknowledged by T.E.M. and A.S., and T.H.J. acknowledges the help from the Norwegian Research Council.

Supporting Information Available: Movies to Figures 4−7 and a derivation of eq 1.

References and Notes

(1) Paxton, W. F.; Kistler, K. C.; Olmeda, C. C.; Sen, A.; St. Angelo, S. K.; Cao, Y.; Mallouk, T. E.; Lammert, P. E.; Crespi, V. H. Catalytic Nanomotors: Autonomous Movement of Striped Nanorods. *J. Am. Chem. Soc.* **2004**, *126*, 13424−13431.

(2) Kline, T. M.; Paxton, W. F.; Mallouk. T. E.; Sen, A.; Catalytic Nanomotors: Autonomous Movement of Striped Metallic Nanorods. *Angew Chem., Int. Ed*. **2005**, *44*, 744−746.

(3) Fourier-Bidoz, S.; Arsenault, A. C.; Manners, I.; Ozin, G. A. Synthetic self-propelled nanorotors. *Chem. Commun.* **2005**, 441−443.

(4) Golestanian, R.; Liverpool, T. B.; Adjari, A. Propulsion of a molecular machine by asymmetric distribution of reaction products. *Phys. Rev. Lett.* **2005**, *94*, 220801, 1−4.

(5) Stone, H. A.; Stroock, A. D.; Ajdari, A. Engineering flows in small devices Microfluidics Toward a Lab-on-a-Chip. *Annu. Rev. Fluid Mech.* **2004**, *36*, 381−411.

(6) Anderson, J. L. Colloidal transport by interfacial forces. *Annu. Rev. Fluid Mech.* **1989**, *21*, 61−99.

(7) Frankel, R. B.; Bazylinski, D. A. Magnetotaxis and Magnetic particles in Bacteria. *Hyperfine Interact*. **1994** *90*, 135−142.

(8) Wajnberg, E.; de Souza Solvo, L. H.; Lins de Barros, H. G. P.; Esquivel, D. M. S. A study of Magnetic properties of Magnetotactic bacteria. *Biophys. J.* **1986** *50*, 451−455.

(9) The power P is calculated as $P = f\eta l v^2$, where f is the frictional coefficient, η is the viscosity of water, l is the length of the rod, and v is the velocity of propulsion.

(10) Bazylinski, D. A.; Frankel, R., B. Magnetosome Formation in Prokaryotes. *Nat. Rev. Microbiol.* **2004**, *2*, 217−230.

(11) In the synthesis of the Fe_3O_4 nanoparticles, we followed the protocole outlined by Sahoo, Y.; Goodarzi, A.; Swihart, M. T.; Ohulchanskyy, T. Y.; Kaur, N.; Furlani, E. P.; Prasad, P. N. Aqueous Ferrofluid of Magnetite Nanoparticles: Fluorescence Labeling and Magnetophoretic Control. *J. Phys. Chem. B.* **2005**, *109*, 3879−3885.

(12) In a magnetic field, the angle alignment φ follows the equation $\varphi = 2 \arctan[\exp mHt/\Gamma]$ where m is the magnetic moment of the rod, t is the time and $\Gamma = \pi\eta L^3/3[\ln(L/R) - 0.8]$ is the viscous rotational friction coefficient with η, the viscosity of water, and L and R, the length and radius of the rod. A fit to the realignment kinetics yields a magnetic moment of 7.8×10^{-18} Am^2 from which we then infer the magnetization by dividing by the volume of the nickel segments.

(13) Paxton, W. F.; Sen, A.; Mallouk, T. E. Motility of Catalytic Nanoparticles through Self-generated forces. *Chem. Eur. J.* **2005**, *11*(22), 6462−6470.

(14) Dhar, P.; Fischer, Th. M.; Wang, Y.; Mallouk, T. E.; Paxton, W. F.; Sen, A. Autonomously Moving Nanorods at a Viscous Interface. *Nanoletters* **2006**, *6*, 66−72.

(15) Wang, Y.; Hernandez, R. M.; Bartlett, D. J., Jr.; Bingham, J. M.; Kline, T. R.; Sen, A.; Mallouk, T. E. A Bipolar Alectrochemical Mechanism for Propulsion of Catalytic Nanomotors in Hydrogen Peroxide Solutions. *Langmuir* **2006**, *22*, 10451−10456.

(16) Shlesinger, M. F.; West, B. J.; Klafter, J. Levy dynamics of enhanced diffusion: application to turbulence. *Phys. Rev. Lett.* **1987**, *58*, 1100−1103.

(17) Heyen, U.; Schuler, D. Growth and Magnetosome Formation by microaerophilic Magnetospirillum strains in an oxygen-controlled fermentor. *Appl. Microbiol. Biotechnol.* **2003**, *61*, 536−544.

(18) Helseth, L. E.; Backus, T.; Johansen, T. H.; Fischer, T. M. Colloid Crystallization and Transport in Stripes and Mazes. *Langmuir* **2005**, *21*, 7518−7523.

(19) The function ψ reads: $\Psi = 2i/\pi\, M/k\, \{di\, \log(1 - e^{ik(x+iz\, \pi/2k\, H_{ex}/M_s)}) - di\, \log(1 + e^{ik(x+iz\, +\, \pi/2k\, H_{ex}/M_s)}) + \pi/2\, k(x + iz)\, H_{ex}/M_s\}$ where the surface of the film is placed at $z = 0$ with the stripe modulation in the x-direction. H_{ex} is the external field and $\pm M_s$ the magnetization of the up and down domains of the film and $di\, \log(w) = -\int_1^w \ln(t)/t - 1\, dt$ denotes the dilogarithmic function. The magnetic field lines are then given by $\mathrm{Im}(\Psi) = const.$

(20) Kalmijn, A. J.; Blakemore, R. P. The Magnetic Behavior of Mud Bacteria. In *Proceedings in Life Science. Animal Migration, Navigation and Homing*; Schmidt-Konig, K., Keeton, W. T., Eds.; Springer-Verlag KG: Berlin, Germany, 1978; pp 354−355.